



Clostridium difficile Alters the Structure and Metabolism of Distinct Cecal Microbiomes during Initial Infection To Promote Sustained Colonization

Matthew L. Jenior,^a Jhansi L. Leslie,^a Vincent B. Young,^{a,b} Patrick D. Schloss^a

^aDepartment of Microbiology and Immunology, University of Michigan, Ann Arbor, Michigan, USA

^bDepartment of Internal Medicine/Infectious Diseases Division, University of Michigan Medical Center, Ann Arbor, Michigan, USA

ABSTRACT Susceptibility to *Clostridium difficile* infection (CDI) is primarily associated with previous exposure to antibiotics, which compromise the structure and function of the gut bacterial community. Specific antibiotic classes correlate more strongly with recurrent or persistent *C. difficile* infection. As such, we utilized a mouse model of infection to explore the effect of distinct antibiotic classes on the impact that infection has on community-level transcription and metabolic signatures shortly following pathogen colonization and how those changes may associate with persistence of *C. difficile*. Untargeted metabolomic analysis revealed that *C. difficile* infection had significantly larger impacts on the metabolic environment across cefoperazone- and streptomycin-pretreated mice, which became persistently colonized compared to clindamycin-pretreated mice, where infection quickly became undetectable. Through metagenome-enabled metatranscriptomics, we observed that transcripts for genes associated with carbon and energy acquisition were greatly reduced in infected animals, suggesting that those niches were instead occupied by *C. difficile*. Furthermore, the largest changes in transcription were seen in the least abundant species, indicating that *C. difficile* may “attack the loser” in gut environments where sustained infection occurs more readily. Overall, our results suggest that *C. difficile* is able to restructure the nutrient-niche landscape in the gut to promote persistent infection.

IMPORTANCE *Clostridium difficile* has become the most common single cause of hospital-acquired infection over the last decade in the United States. Colonization resistance to the nosocomial pathogen is primarily provided by the gut microbiota, which is also involved in clearing the infection as the community recovers from perturbation. As distinct antibiotics are associated with different risk levels for CDI, we utilized a mouse model of infection with 3 separate antibiotic pretreatment regimens to generate alternative gut microbiomes that each allowed for *C. difficile* colonization but varied in clearance rate. To assess community-level dynamics, we implemented an integrative multi-omics approach that revealed that infection significantly changed many aspects of the gut community. The degree to which the community changed was inversely correlated with clearance during the first 6 days of infection, suggesting that *C. difficile* differentially modifies the gut environment to promote persistence. This is the first time that metagenome-enabled metatranscriptomics have been employed to study the behavior of a host-associated microbiota in response to an infection. Our results allow for a previously unseen understanding of the ecology associated with *C. difficile* infection and provide the groundwork for identification of context-specific probiotic therapies.

KEYWORDS 16S rRNA gene sequencing, *Clostridium difficile*, colonization resistance, machine learning, microbiome, systems biology, metabolomics, metagenomics, metatranscriptomics, microbial ecology


Received 10 May 2018 Accepted 4 June 2018 Published 27 June 2018

Citation Jenior ML, Leslie JL, Young VB, Schloss PD. 2018. *Clostridium difficile* alters the structure and metabolism of distinct cecal microbiomes during initial infection to promote sustained colonization. mSphere 3:e00261-18. <https://doi.org/10.1128/mSphere.00261-18>.

Editor Susannah Green Tringe, DOE Joint Genome Institute

Copyright © 2018 Jenior et al. This is an open-access article distributed under the terms of the [Creative Commons Attribution 4.0 International license](https://creativecommons.org/licenses/by/4.0/).

Address correspondence to Patrick D. Schloss, pschloss@umich.edu.

 *Clostridium difficile* alters the structure and function of the murine microbiome during initial infection to promote sustained colonization. @PatSchloss

One of the many beneficial functions provided by the indigenous gut bacterial community is its ability to protect the host from infection by pathogens (1). This attribute, termed colonization resistance, is one of the main mechanisms that protect healthy individuals from the gastrointestinal pathogen *Clostridium difficile* (2–4). *C. difficile* infection (CDI) is responsible for most cases of antibiotic-associated colitis, a toxin-mediated diarrheal disease that has dramatically increased in prevalence over the last 10 years. There are an estimated 453,000 cases of CDI resulting in 29,000 deaths in the United States annually (5). Antibiotics are a major risk factor for CDI and are thought to increase susceptibility by disrupting the gut bacterial community structure; however, it is still unclear what specific changes to the microbiota contribute to this susceptibility (6, 7). Although most classes of antibiotics have been associated with initial susceptibility to CDI, fluoroquinolones, clindamycin, and cephalosporins are linked to increased risk of recurrent or persistent infection (8–10). This raises questions about the groups of bacteria that are differentially impacted by certain therapies and how these changes affect the duration or severity of the infection.

Associations between the membership and functional capacity of the microbiota as measured by the metabolic output suggest that antibiotics increase susceptibility by altering the nutrient milieu in the gut to one that favors *C. difficile* metabolism (11–13). One hypothesis is that *C. difficile* colonization resistance is driven by competition for growth substrates by an intact community of metabolic specialists. This has been supported by animal model experiments over the past several decades (14–16). This line of reasoning has been carried through to the downstream restoration of colonization resistance with the application of fecal microbiota transplant (FMT). Although an individual's microbiota may not return to its precise original state following FMT, it is hypothesized that the functional capacity of the new microbiota is able to outcompete *C. difficile* for resources and clear the infection (13, 17).

Leveraging distinct antibiotic treatment regimens in a murine model of CDI (18), we and others have shown that *C. difficile* adapts its physiology to the distinct cecal microbiomes that resulted from exposure to antibiotics (18, 19). We went on to show that *C. difficile* appears to adapt portions of its metabolism to fit alternative nutrient niche landscapes. As the diet of the mice remained unchanged, changes in the cecal metabolome are likely driven by the intestinal microbiota. Although it has been established that *C. difficile* colonizes these communities effectively, it is unknown whether the differences in the metabolic activity of communities following antibiotic treatment are impacted by *C. difficile* colonization or if they correlate with prolonged infection. Historically, it has been difficult to ascribe specific metabolic contributions to individual taxa within the microbiota during perturbations, especially within the context of a host. To address this limited understanding, we employed an integrative untargeted metabolomic and metagenome-enabled metatranscriptomic approach to investigate specific responses to infection of the gut microbiota in a murine model of CDI. This high-dimensional analysis allowed us not only to characterize the metabolic output of the community but also to identify which subgroups of bacteria were differentially active during mock infection and CDI. Our results supported the hypothesis that CDI was indeed associated with altered community-level gene transcription and metabolomic profile of susceptible environments. This effect was significantly more pronounced in communities where *C. difficile* was able to maintain colonization. This work highlights the need for increased appreciation of the differential, combined effects of antibiotics and CDI on the gut microbiota to develop more successful targeted therapies that eliminate *C. difficile* colonization.

RESULTS

Distinct antibiotic pretreatments are associated with alternative community structures that are equally susceptible to initial *C. difficile* colonization but differ in patterns of clearance. We have previously shown that when conventionally reared specific-pathogen-free (SPF) mice were pretreated with one of three different antibiotics (streptomycin, cefoperazone, and clindamycin) (see Table S1 in the supplemental

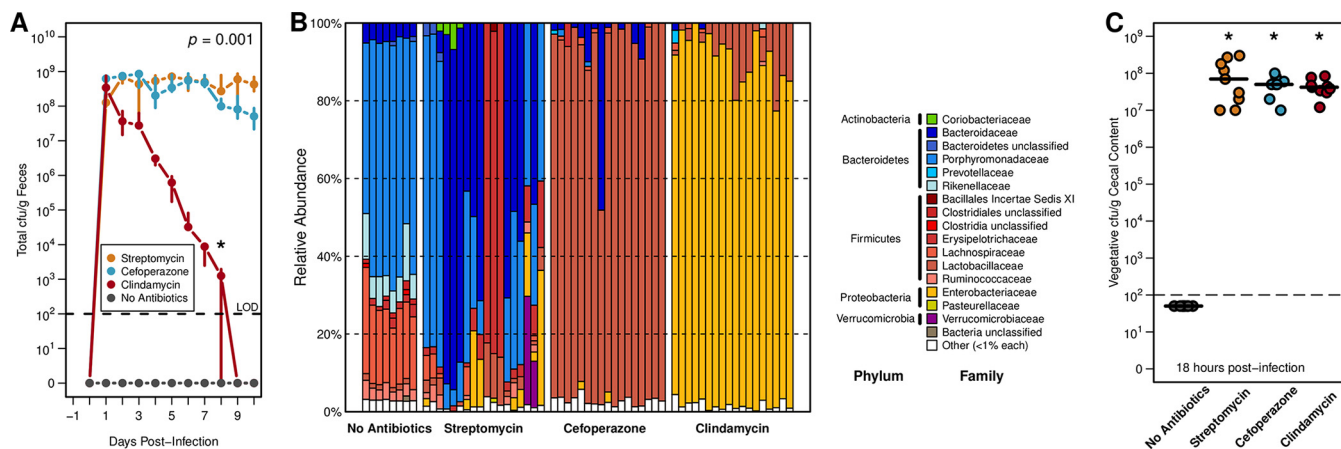


FIG 1 Distinct antibiotic pretreatments have differential impacts on *C. difficile* colonization and cecal microbiota community structure. (A) CFU of *C. difficile* 630 in stool of infected mice following each antibiotic-pretreated group over 10 days of infection. Median and interquartile range are shown for each time point. Both cefoperazone and streptomycin pretreatments had more significantly detectable CFU on the final day than did clindamycin pretreatment ($P < 0.001$). (B) Relative abundance of family-level OTU taxonomic classification in each pretreatment group from 16S rRNA gene sequencing. (C) Quantification of terminal vegetative *C. difficile* CFU in cecal content across 18-h colonization models. Black lines indicate median values, and each pretreatment group had significantly greater detectable CFU than no-antibiotic controls. Significant differences in panel A were determined through permutational multivariate analysis of variance (PERMANOVA) with dynamic time warping, and those in panel C were found by Wilcoxon rank sum test with Benjamini-Hochberg correction when necessary. The limit of detection (LOD) was used in place of undetectable values for statistical testing.

material), each pretreatment was associated with altered patterns of *C. difficile* virulence factor expression (19). These antibiotics were chosen not only for the ability to reduce *C. difficile* colonization resistance in a mouse model (18) but also for distinct and significant impacts on the structure and diversity of the cecal microbiota (Fig. 1A) (19). In each antibiotic pretreatment, we observed equally high levels of *C. difficile* colonization on the day after infection; however, over the subsequent 9 days clindamycin-pretreated mice were the only mice in which the amount of *C. difficile* in the feces fell below the limit of detection, while mice receiving the other pretreatments remained highly colonized ($P = 0.01$) (Fig. 1A). We hypothesized that this occurred in the clindamycin-pretreated mice because the perturbed intestinal community occupied niche space that overlapped that of *C. difficile*.

We chose to focus our remaining experiments on cecal samples collected 18 h after infection to assess the behavior of *C. difficile* directly prior to the reduction in detectable *C. difficile*. This endpoint corresponded with that in a previous study where *C. difficile* reached maximum cecal vegetative cell load with few detectable spores (20). We also elected to examine cecal content because the cecum was more likely than stool to be a site of active bacterial metabolism and would allow for an assessment of functional differences in the microbiota. At 18 h after infection, we found that the communities remained highly differentiated from untreated controls as measured by 16S rRNA gene sequencing of the V4 region (Fig. 1B). The composition of streptomycin-pretreated communities was more variable between cages but was generally enriched for members of the *Bacteroidetes* phylum. Cefoperazone- and clindamycin-pretreated cecal communities were consistently dominated by members of the *Lactobacillaceae* and *Enterobacteriaceae* families, respectively. Despite variation in the community structures, there were no significant differences in the number of vegetative cells among any of the antibiotic pretreatment groups (Fig. 1C). All susceptible mice were colonized with $\sim 1 \times 10^8$ vegetative CFU per gram of cecal content, and untreated mice maintained *C. difficile* colonization resistance.

Multiple biological signatures in the bacterial community and metabolome differentiated cecal microbiomes that remained colonized by *C. difficile* from those that did not. Pretreatment with antibiotics not only alters the structure of the resident microbiota but also has a dramatic impact on the intestinal metabolome (11–13). To understand the ramifications that each antibiotic had on the cecal metabo-

lomic environment, we performed untargeted metabolomic analysis on the cecal contents that were also utilized in the 16S rRNA gene sequencing. We identified a total of 727 distinct metabolites. In combination with our 16S rRNA gene sequencing results, we first characterized the differences between the microbiomes (i.e., the microbiota, plus the associated metabolome) of the mock-infected animals to quantify possible drivers of communities that cleared the infection. To focus our analysis on ascertaining changes in discrete populations within the microbiota, we generated operational taxonomic units (OTUs) clustered at 97% similarity. We also removed all *C. difficile* 16S rRNA gene sequences, which represented an average of 2.113% of sequencing reads across infection groups, to eliminate their direct impact in downstream calculation. Using these methods, we discovered that the Bray-Curtis dissimilarities of both the community structure ($P < 0.001$) and the metabolome ($P < 0.001$) were significantly different between cleared and colonized groups during the early stages of infection (Fig. 2A and C). These results supported the hypothesis that the cecal environment created by clindamycin pretreatment was highly divergent from the other groups and likely contributed to the clearance seen in the subsequent days.

To identify the populations and metabolites that were associated with sustained colonization, we utilized Random Forest machine learning with cross-validation to identify the smallest optimal subset of features that could successfully differentiate microbiomes associated with infection clearance and those that remain colonized (21). We identified a model with 5 OTUs that correctly classified all samples to their corresponding groups (Fig. 2B) (out-of-bag error = 0%). Interestingly, these OTUs were not consistently abundant in antibiotic-pretreated communities. Similarly, when we used the same approach with the metabolomic data, we identified a model that used 5 metabolites that correctly differentiated the groups (Fig. 2D) (out-of-bag error = 0%). Together, these results further supported the hypothesis that the environment of the cecum, even early during infection, is distinct between groups that clear the infection and those that maintain *C. difficile* at high levels. Furthermore, results from machine learning analysis suggest that rare members of the communities had a disproportionate influence on the clearance patterns observed between pretreatment regimens and that changes in community structure may be less consistent than changes in the metatranscriptome or metabolome.

Amino acid metabolism by *C. difficile* appears important for sustained colonization across susceptible environments. The ability of *C. difficile* to metabolize amino acids via Stickland fermentation may be a critical nutrient niche that enables it to colonize some perturbed communities (22). We were curious whether this behavior was conserved across multiple distinct gut environments where *C. difficile* was able to colonize. We assessed the changes between the antibiotic-pretreated, mock-infected microbiomes and those of untreated, *C. difficile*-resistant animals. Not only were the relative abundances of Stickland fermentation substrates increased across susceptible environments, but several secondary bile acids which have been shown to be negatively correlated with *C. difficile* susceptibility were significantly decreased (Fig. S1D) ($P < 0.001$). Additionally, when we constructed a Random Forest classification model to differentiate the groups, we identified multiple members of the *Clostridia* which are capable of metabolizing amino acids for growth (23). The relative abundances of these populations were significantly lower in susceptible animals (Fig. S1B) ($P < 0.001$). We also performed a similar analysis to investigate changes induced by *C. difficile* colonization itself in these susceptible conditions. Although CDI alone did not induce significant shifts in the global community structure or metabolome (Fig. S2A and C) ($P = 0.185$ and 0.065 , respectively), several features were able to discriminate infected and uninfected microbiomes with high accuracy. This analysis highlighted numerous growth substrates that are known for *C. difficile* in all pretreated mice, including 6 Stickland substrates, 4 of which were proline conjugates, along with arabinonate/xylonate (Fig. S2D). Furthermore, 5-aminovaleate, the most common end product of Stickland fermentation, was significantly increased during infection in almost all of the metabolomes. Inspection of these specific metabolites revealed that clindamycin pre-

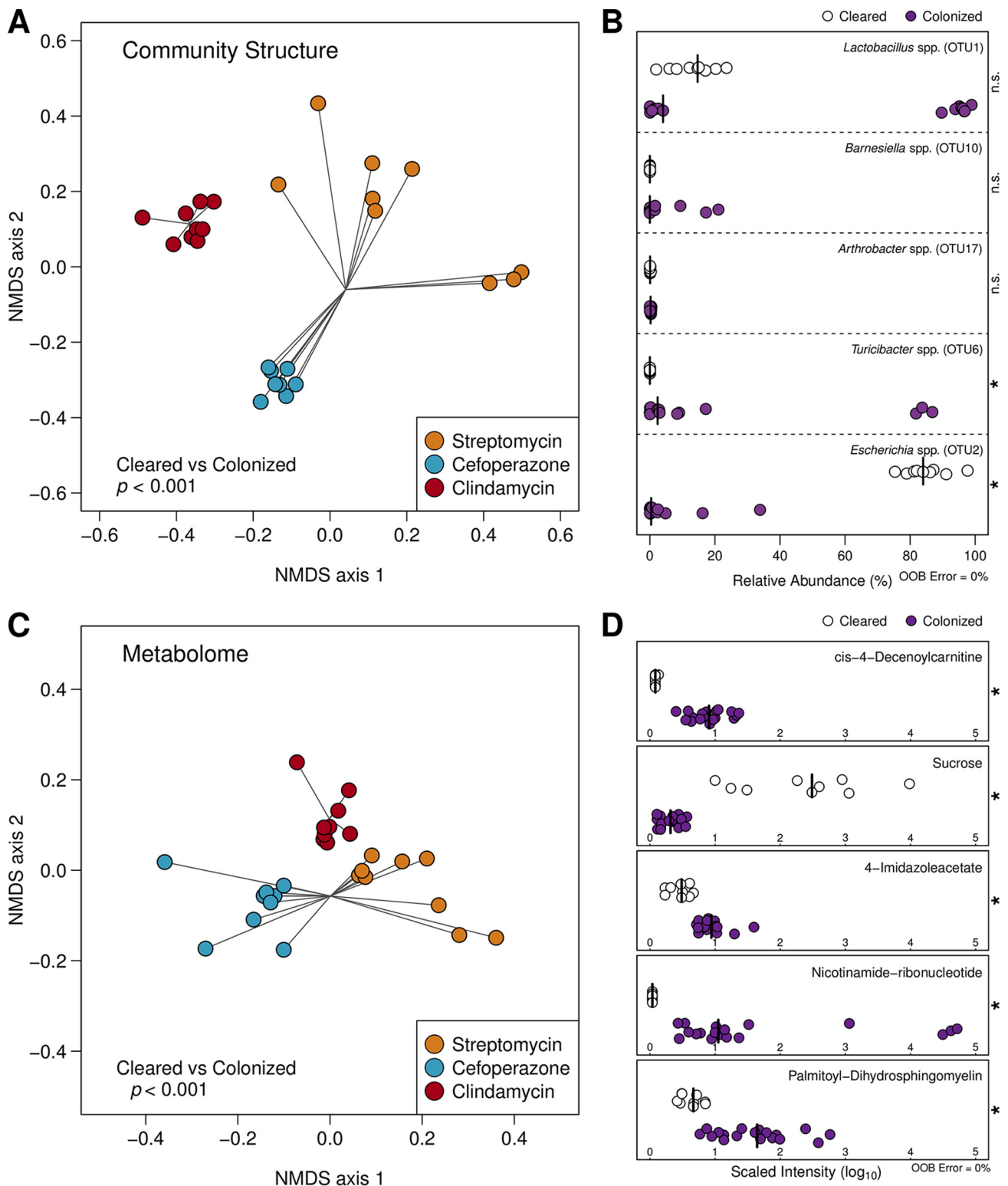


FIG 2 Significant differences in cecal community structure and metabolomes track with downstream *C. difficile* clearance across antibiotic pretreatment regimens. (A) Nonmetric multidimensional scaling (NMDS) ordination of Bray-Curtis distances of OTU relative abundances between mouse cecal communities that remained colonized by *C. difficile* and those that eventually cleared the infection. (B) Relative abundance of OTUs included the optimal model generated by AUCRF classifying the same groups as in panel A. Species-level identification was obtained using centroid representative sequences for each OTU. (C) NMDS ordination of Bray-Curtis distances using metabolite intensities between the abovementioned groups of animals. (D) Scaled intensity of metabolites included the optimal model generated by AUCRF classifying colonized and clearing mouse cecal microbiomes. Differences for ordinations in panels A and C were calculated using PERMANOVA. Optimal AUCRF models demonstrated 0% out-of-bag (OOB) error, and significant differences in panels B and D were determined by Wilcoxon rank sum test with Benjamini-Hochberg correction.

treatment was the only condition under which both the inputs and outputs of Stickland fermentation were less abundant than in the untreated mice (Fig. S3).

Infection corresponded with larger shifts in the metatranscriptomes of communities that allowed sustained *C. difficile* colonization. Despite the strong associations between bacterial community structure and the metabolome with colonization resistance, it was difficult to associate specific populations with changes in those metabolites that were associated with the duration of infection. To gain a more specific understanding of how the microbiota or *C. difficile* shaped the metabolic environment, we employed parallel metagenomic and metatranscriptomic shotgun sequencing of the samples collected from the cecal content of the mice used in the previous analyses. To achieve usable concentrations of bacterial mRNA after rRNA depletion, we had to pool the samples within each treatment and infection group. To establish confidence in the results of a pooled analysis, we calculated within-group sample variance among replicates using CFU, OTU relative abundance, and metabolomic relative abundance data (Table S3). These analyses revealed low levels of variance within control and experimental groups. Following sequencing, metagenomic reads from mock-infected cecal communities were assembled *de novo* into contigs, and putative genes were identified, resulting in 234,868 (streptomycin), 83,534 (cefoperazone), and 35,681 (clindamycin) open reading frames in each metagenome. Of these putative genes, 28.5% could be annotated to a known function based on the KEGG database, and many of these annotations were homologs to genes in species that were found in our data set. Streptomycin pretreatment resulted in a significantly more diverse community than other groups based on 16S rRNA gene sequence data, so a more diverse metagenome was expected (Table S1). Supporting this prediction, 2,408 unique functionally annotated genes were detected in the streptomycin pretreatment metagenome, at least 1,163 more genes than were found in either the cefoperazone or clindamycin metagenome (Fig. S4A to D). Metagenome-enabled mapping of the metatranscriptomic reads revealed that we were able to obtain informative depths of sequencing from across the metagenomic libraries (Fig. S4E and F). As expected, genes with any detectable transcript in any metatranscriptome were a subset of their corresponding metagenome. Metatranscriptomic read abundances were normalized to corresponding metagenomic coverage per gene to normalize for the abundance of the contributing bacterial taxa. This step was followed by a final subsampling of reads from each condition to control for uneven sequencing effort and to identify genes with the largest changes in transcription relative to uninfected animals.

We hypothesized that the degree of change in the metatranscriptome corresponding with *C. difficile* colonization would reflect the shifts seen in the metabolome. As disparate bacterial taxa possess vastly different metabolic capabilities and the antibiotic pretreatments induced distinct species profiles in each community, we tested our hypothesis by delineating the transcriptomic contributions of separate bacterial taxa within each metatranscriptome. Since many genes lack a specific functional annotation in KEGG but retain general taxonomic information, we continued the analysis at the genus level of classification for all genes contributed to each metagenome. Using this approach, we directly compared the normalized transcript abundances for each gene between infected and uninfected states for each antibiotic pretreatment and calculated the Spearman correlation to identify distinct patterns of transcription (Fig. 3). This resulted in 2,473 genes that had an average distance from the center of 2.545 associated with streptomycin pretreatment, 2,930 genes at an average distance of 3.854 in cefoperazone pretreatment, and only 727 genes at an average distance of 2.414 with clindamycin pretreatment. Overall, the clindamycin pretreatment was associated with the fewest transcription outliers between uninfected and infection conditions compared with those of the other antibiotic groups. This suggested that the degree to which the metatranscriptome was altered by infection corresponded to prolonged colonization.

This analysis also revealed that outlier genes originated in underrepresented genera. In streptomycin-pretreated mice, 937 genes belonging to *Lactobacillus* were increased

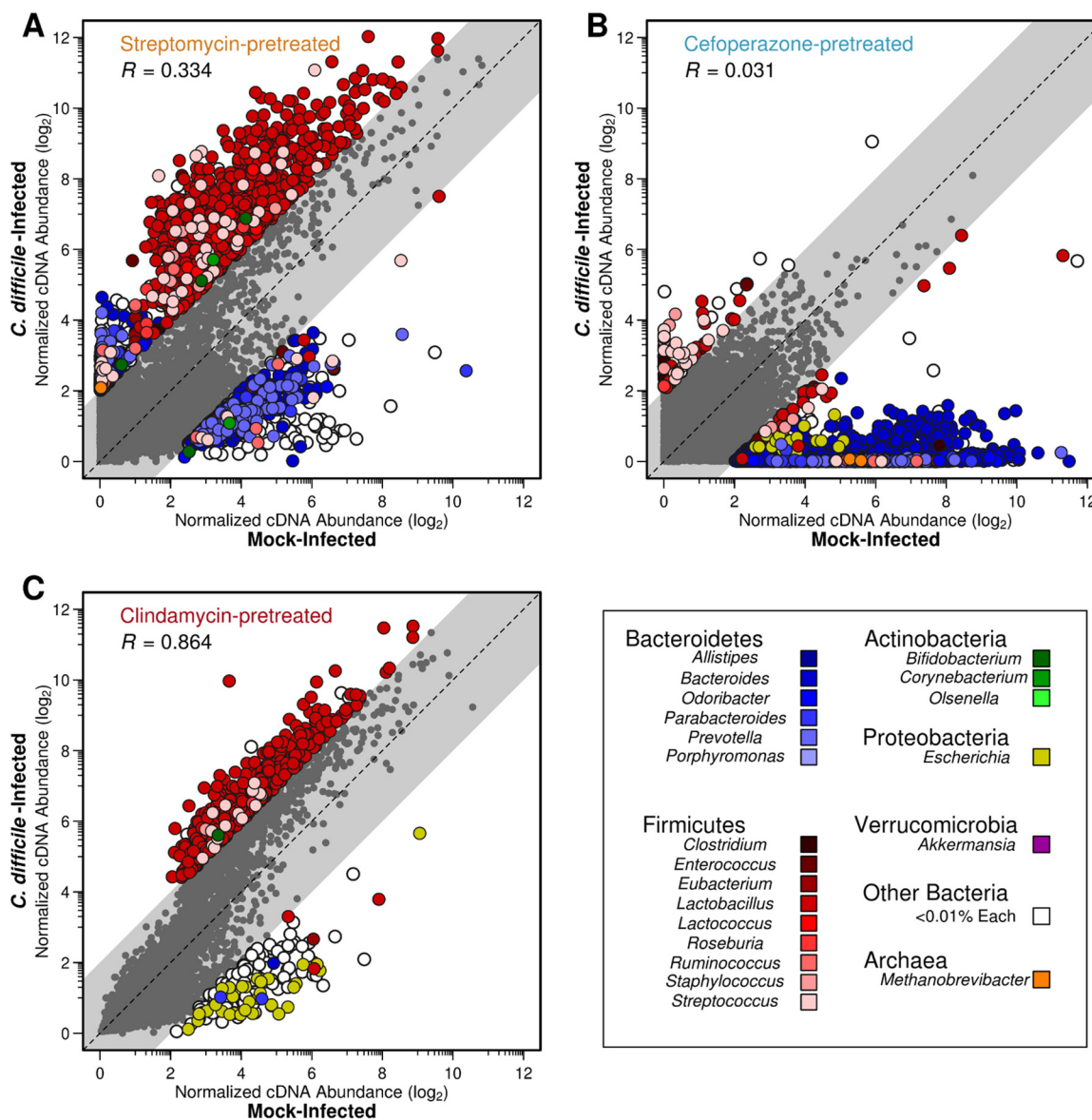


FIG 3 *C. difficile* colonization alters gene transcription of taxonomic groups differentially between antibiotic pretreatments. Each point represents a unique gene from the respective metagenomic assembly. Coordinates were determined by the \log_2 -transformed difference in transcription level between *C. difficile*-infected and mock-infected conditions for each gene. Outliers were defined using linear correlation and a squared residual cutoff of 2. Euclidean distance of outliers to the $x = y$ line was also calculated. The coloring of each point indicates the genus from which the transcript originated, and the gray points denote those genes with consistent transcription levels between conditions as defined by outlier analysis. Antibiotic pretreatments: streptomycin (A), cefoperazone (B), and clindamycin (C).

in transcription during *C. difficile* infection, where *Lactobacillus* accounted for 0.42% of the 16S rRNA gene sequences (Fig. 3A). In cefoperazone-pretreated mice, 2,290 genes belonging to *Bacteroides* had lower transcription during *C. difficile* infection; *Bacteroides* accounted for 1.49% of the 16S rRNA gene sequences (Fig. 3B). A consistent trend in streptomycin- and cefoperazone-pretreated mice was an overrepresentation of highly transcribed genes from genera belonging to *Bacteroidetes* during mock infection. The metatranscriptomes among mice from both of these pretreatment conditions poorly correlated between mock and infected conditions, indicating a high degree of change induced by *C. difficile* colonization ($R = 0.334$ and $R = 0.031$, respectively). In clindamycin-pretreated mice, the largest difference in transcription was for 510 *Lactobacillus* genes with increased transcription during CDI; *Lactobacillus* accounted for 2.7% of the 16S rRNA gene sequences (Fig. 3C). Infected and uninfected metatranscriptomes

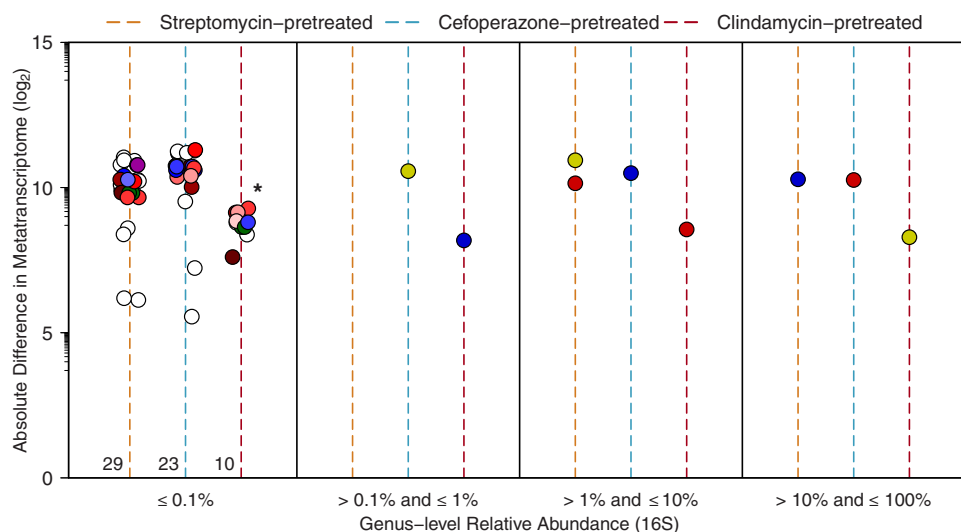


FIG 4 A majority of metatranscriptomic changes are focused within minority members of each microbiota. Absolute difference in metatranscriptomic reads contributed by each genus in pretreatments between mock- and *C. difficile*-infected conditions. Colored lines denote antibiotic pretreatment. Each point represents all transcripts contributed by that genus in each pretreatment group, and point colors correspond to those used in Fig. 3. Numbers at the base of pretreatment lines in the first panel represent the quantity of genera in each group, as some points are obscured.

from mice pretreated with clindamycin were more strongly correlated with each other than with either of the other pretreatments ($R = 0.864$). This suggests that although *C. difficile* altered the streptomycin- and cefoperazone-pretreated communities in which it was able to remain stably colonized, it had minimal impact on the clindamycin-pretreated community in which it was not able to remain colonized.

The largest changes in metatranscriptomes in response to infection were concentrated in low-abundance taxa of each pretreatment group. To explore the observation that rare taxa were responsible for the largest differences in transcription in response to infection, we tabulated the absolute difference between mock- and *C. difficile*-infected transcriptomes for each genus in each antibiotic pretreatment. We further normalized these values for the number of genes detected in each genus to adjust for genera that were more successfully assembled or annotated, and we eliminated genera where fewer than 50 genes were detected in the metatranscriptome. Taxa were then stratified into categories based on their relative abundance in each community from 16S rRNA gene sequencing (Fig. 4). This revealed that most change occurred among the rare genera and that the degree of change was inversely correlated with sustained colonization (same colors denoting genera as in Fig. 3). To this point, minority metatranscriptomic absolute differences were significantly reduced in clindamycin pretreatment ($P < 0.001$). Additionally, the proportions of taxa in the lowest-relative-abundance bracket were similar across pretreatment groups (~88.9%). As a corollary, we predicted that the majority of unique genes or metabolic potential was held within this minority, and following quantification, this proved to be the case (Table S4). As a consequence, the downstream impacts on functionality may have a disproportionately large effect on the overall environment of the intestine as a function of its collective metabolism.

Altered transcription within low-abundance taxa favors reduced nutrient competition with *C. difficile* in communities that permit sustained colonization. Based on our metabolomic and metatranscriptomic results, we hypothesized that pathways with the greatest differences between mock- and *C. difficile*-infected mice would be related to catabolism of metabolites that *C. difficile* could use for growth. To assess these changes, we identified those annotated transcripts that were associated with genera that represented less than 0.1% of the community as measured with our 16S

rRNA gene sequence data (Fig. 5). This resulted in the identification of 585 genes that were differentially transcribed between clindamycin-pretreated mice and the streptomycin- and cefoperazone-pretreated mice. From this group of genes, we filtered the collection to identify those genes that were unique to either the clindamycin-pretreated mice or the streptomycin- and cefoperazone-pretreated mice. Finally, we limited our analysis to those genes that were meaningfully different between the mock- and *C. difficile*-infected groups in each antibiotic pretreatment group. This resulted in 34 genes from 11 pathways. These genes and pathways were primarily involved in simple carbohydrate-containing molecule acquisition/utilization (Fig. 5). Interestingly, many of these genes had decreased transcription during infection compared to mock-infected controls. At the pathway level, many genes associated with acquisition of galactose and amino sugar (both *C. difficile* growth substrates) were reduced during infection in both streptomycin- and cefoperazone-pretreated mice. Conversely, pathways uniquely associated with clindamycin-pretreated communities were related to the metabolism of a diverse array of carbon sources, which may indicate ineffective competition by *C. difficile* with this community for any particular growth substrate. Our results indeed suggest that *C. difficile* colonization induces a shift in transcriptional activity for a minority subset of species, possibly in an effort to segregate a desired nutrient niche, prior to the introduction of the hallmark disease phenotypes associated with CDI.

DISCUSSION

Our results demonstrate that distinct intestinal ecosystems are differentially impacted by *C. difficile* colonization and that these changes to community metabolism could have implications for the ability of the pathogen to persist in those environments. We had previously demonstrated that *C. difficile* spore production and toxin activity differ between these pretreatment regimens (19). As both processes have been linked to environmental concentrations of specific growth nutrients (24), these results suggested that despite high initial *C. difficile* colonization, the microbiomes across pretreatments may vary in available nutrients or profiles of competitors for those niches. In the current study, our multi-omics approach demonstrated that *C. difficile* manipulated the niche landscape of the intestinal tract. Instances of active nutrient niche restructuring in the gut have been documented previously for prominent symbiotic bacterial species in gnotobiotic mice (25) but not in a conventionally reared animal model of infection following antibiotic pretreatment. Interestingly, the taxonomic groups that produced the transcripts that were most altered by *C. difficile* colonization were rare in their cecal community. Previous studies have found that rare taxonomic groups, even those at a low abundance as a result of a spontaneous perturbation, may have disproportionate effects on the metabolome of the rest of the community (26). For example, in temperate lakes, conditionally rare microbes were found to be far more metabolically active than highly abundant taxa (27). These examples of responses to perturbations are interesting models for thinking about the dynamics of bacterial populations recovering from an antibiotic perturbation. As such, *C. difficile* may compete with these organisms to ultimately effect greater change in the entire ecosystem and open a long-lasting nutrient niche. While this hypothesis requires further exploration, it provides an ecological framework to study the interactions between *C. difficile* and members of susceptible communities.

This study is one of the first *in vivo* observations that a medically relevant bacterial pathogen may alter the metabolic activity of a host-associated community to promote its own colonization. This is also the first application of metatranscriptomic analysis of the gut microbiota *in vivo* and in response to a pathogen. Other groups have identified potential metabolite markers of *C. difficile* infection in patient feces (28), but they were not able to identify associations with changes in community metabolism that were afforded to us by our paired metabolomic and metatranscriptomic analyses. In a recent study, a tick-vector bacterial pathogen altered the ability of the resident microbiota of the tick by interrupting proper biofilm formation and allowing lasting colonization (29). It was also recently found that bacterial metabolic generalists may be more likely

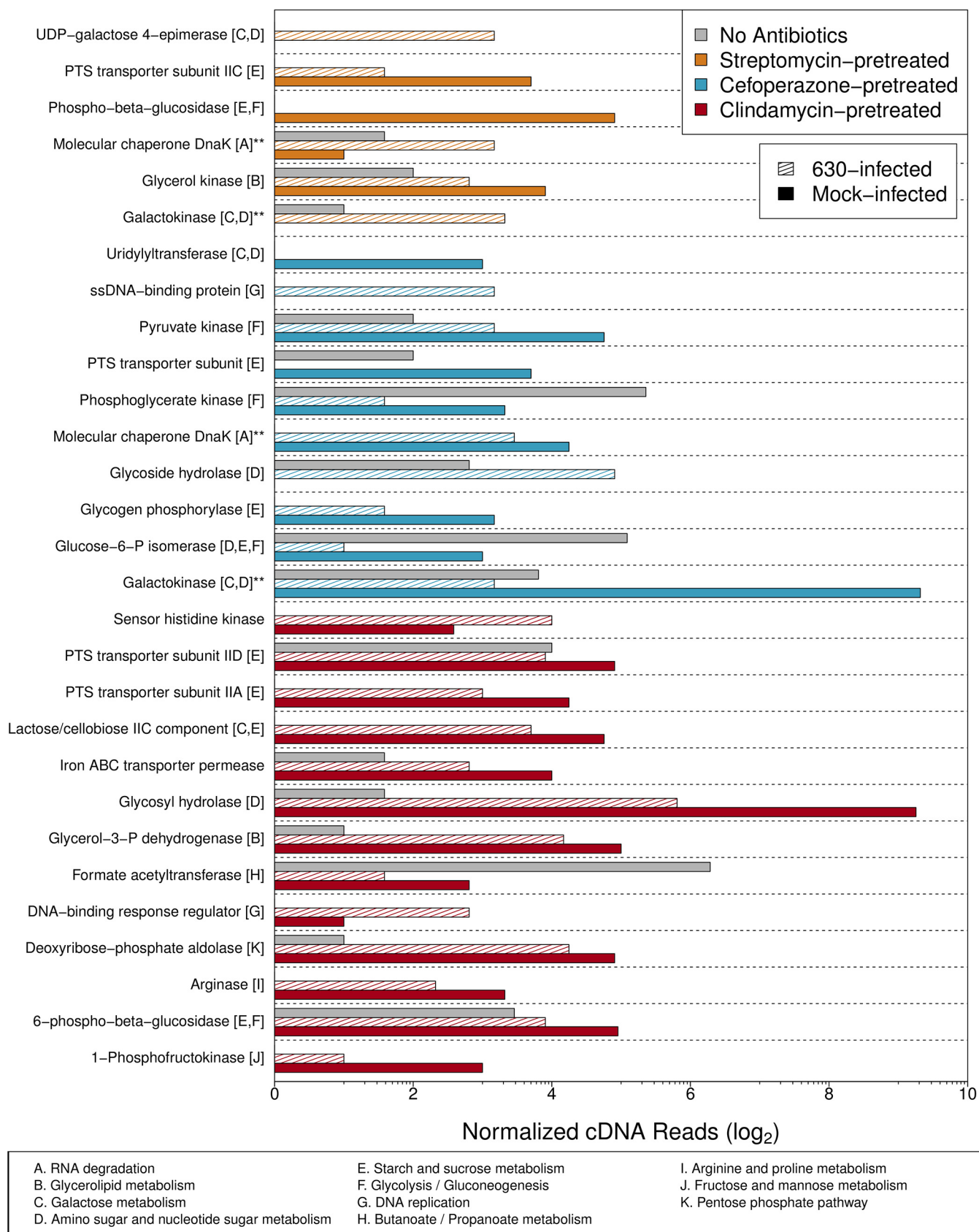


FIG 5 Metatranscriptomic changes due to infection in certain metabolic pathways are overrepresented in the minority taxa. Log₂ metagenome-normalized cDNA abundances for genes with differential transcription during infection belonging to genera that had a relative abundance greater than 0.1%. Double asterisks denote genes shared between pretreatment groups. PTS, phosphotransferase system; ssDNA, single-stranded DNA.

to actively antagonize the growth of other species in an environment that they are colonizing (30). We previously showed that *C. difficile* has a wide nutrient niche space *in vivo* where it most likely utilizes its role as a metabolic generalist to colonize diverse gut microbiomes (19). The ability to simultaneously antagonize the metabolism of surrounding populations in cecal environments that support persistence would explain the more significant shifts in those metatranscriptomes. While we acknowledge that this study may not elucidate the specific mechanism by which this interaction occurs, the combined systems analysis strengthens each individual level of observation. Combining the results from these approaches reveals a clearer understanding of *C. difficile*-related microbial ecology. This research lays the groundwork for a more rational consideration of the metabolic functionalities of bacterial taxa when attempting to rebuild *C. difficile* colonization resistance across differentially perturbed gut environments.

In spite of consistent results across the different methods that we used in this study, several limitations should be noted. First, as with all transcriptomic studies, the relative level of mRNA detected for a given gene does not necessarily reflect the amount of functional protein made by a cell or the posttranslational modifications that are required to activate the enzymes. Additionally, due to the low relative abundance of *C. difficile* in these communities, it was necessary for us to pool samples to generate a large number of reads from each group rather than sampling multiple replicates within each group. Greater transcript read abundance per gene allowed for improved surveillance for the activity of low-abundance species as well as greater confidence in genes found to be highly transcribed. Although the lack of animal-based replication for the metatranscriptomic data does potentially limit the ability to generalize our results, this approach has been successfully utilized by numerous groups in the past to accurately characterize transcriptional activity across communities of bacteria (19, 31–33). Furthermore, the metatranscriptomic data were supported by the 16S rRNA gene sequence and metabolomic data which were collected from individual animals. With respect to the metabolomic data, alternative interpretations of the data also exist. For example, we assumed that metabolites which did not change in concentration between uninfected and infected conditions were not impacted by *C. difficile* colonization. However, it is possible that the metabolism of *C. difficile* itself simply substituted for a function that was already present in the uninfected community. The insights gathered from the metatranscriptomic data suggest that this was unlikely. By leveraging multiple methods to test our hypotheses, we were able to mediate the weaknesses of any individual method and present a more unified description of the system than any of the methods on their own.

Our study supports the hypothesis that the gut microbiota of healthy individuals maintains colonization resistance to *C. difficile* by outcompeting the pathogen for preferred nutrient niche space. Moreover, these data suggest that the degree to which the environment of the intestine is altered by infection may be linked to the ability of the pathogen to remain colonized. Ultimately, our results suggest that each susceptible and subsequently infected microbiome may be unique and require specific microbes or functionalities to restore colonization resistance against *C. difficile* in that specific context. Conversely, colonization resistance against *C. difficile* may be the result of contributions by distinct subcommunities of bacteria across each unique resistant gut community. Several studies have attempted to identify single bacterial species or consortia that are able to achieve colonization resistance; however, these efforts have resulted in only partial resistance (34–37). Considering that the structure and function of the microbiome are intimately connected to colonization resistance to *C. difficile*, it has become imperative to understand the ecological factors that allow some gut environments to be persistently colonized while others are not. This research lays the groundwork for future studies to assess context-dependent restoration of *C. difficile* colonization resistance and what factors are able to interfere with the ability of *C. difficile* to modify gut ecology to promote clearance.

MATERIALS AND METHODS

Animal care and antibiotic administration. Briefly, approximately equal numbers of male and female conventionally reared 6- to 8-week-old C57BL/6 mice were randomly assigned to each experimental group (sexes were housed separately). Nine mice were used per experimental/control condition, and littermates were used as much as possible within each group to account for possible genetic variability. They were administered one of three antibiotics, cefoperazone, streptomycin, or clindamycin, before oral *C. difficile* infection (see Table S1 in the supplemental material). A detailed description of these animal models was outlined previously (19). A similar experimental design was implemented for gnotobiotic mice and was performed with the University of Michigan Germfree Mouse Center as described previously (19). All animal protocols were approved by the University Committee on Use and Care of Animals at the University of Michigan and carried out in accordance with the approved guidelines from the Office of Laboratory Animal Welfare (OLAW), United States Department of Agriculture (USDA) registration, and the Association for Assessment and Accreditation of Laboratory Animal Care (AAALAC). The protocol license Institutional Animal Care and Use Committee (IACUC) number for all described experiments is PRO00006983.

C. difficile infection and necropsy. On the day of challenge, 1×10^3 *C. difficile* spores were administered to mice via oral gavage in phosphate-buffered saline (PBS) vehicle. Mock-infected animals were given an oral gavage of 100 μ l PBS at the same time as those mice administered *C. difficile* spores. Eighteen hours following infection, mice were euthanized by CO₂ asphyxiation and necropsied to obtain the cecal contents. Aliquots were immediately flash frozen for later DNA extraction. A third aliquot was transferred to an anaerobic chamber for quantification of *C. difficile* abundance. The remaining content in the ceca was mixed in a stainless steel mortar housed in a dry ice and ethanol bath. Cecal contents from all mice within each pretreatment group were pooled into the mortar prior to grinding to a fine powder. The ground content was then stored at -80°C for subsequent RNA extraction. For 10-day colonization studies, fresh stool was collected from infected mice each day beginning on the day of infection. Mice were monitored for overt signs of disease and were euthanized after the final stool collection.

C. difficile cultivation and quantification. Cecal samples were weighed and serially diluted under anaerobic conditions with anaerobic PBS. Differential plating was performed to quantify *C. difficile* vegetative cells by plating diluted samples on CCFAE plates (fructose agar plus cycloserine, cefoxitin, and erythromycin) at 37°C for 24 h under anaerobic conditions (38). Quantification of total *C. difficile* CFU for the 10-day colonization experiments was performed from stool using TCCFAE to measure total *C. difficile* load in these animals over time.

DNA/RNA extraction and sequencing library preparation. DNA for shotgun metagenomic and 16S rRNA gene sequencing was extracted from approximately 50 mg of cecal content from each mouse using the PowerSoil-htp 96-well soil DNA isolation kit (Mo Bio Laboratories) and an EpMotion 5075 automated pipetting system (Eppendorf). The V4 region of the bacterial 16S rRNA gene was amplified using custom barcoded primers (39). Equal molar ratios of raw isolated DNA within each treatment group were then pooled, and ~ 2.5 ng of material was used to generate shotgun libraries with a modified 10-cycle Nextera XT genomic library construction protocol (Illumina). This was done to mimic the pooling strategy necessary for metatranscriptomic library preparation. Final libraries were pooled at equal molar ratios and stored at -20°C . For RNA extraction, a more detailed description of the procedure can be found in reference 19. Briefly, immediately before RNA extraction, 3 ml of lysis buffer (2% SDS, 16 mM EDTA, and 200 mM NaCl) contained in a 50-ml polypropylene conical tube was heated for 5 min in a boiling water bath (40). The hot lysis buffer was added to the frozen and ground cecal content. The mixture was boiled with periodic vortexing for another 5 min. After boiling, an equal volume of 37°C acid phenol-chloroform was added to the cecal content lysate and incubated at 37°C for 10 min with periodic vortexing. The mixture was then centrifuged at $2,500 \times g$ at 4°C for 15 min. The aqueous phase was then transferred to a sterile tube, and an equal volume of acid phenol-chloroform was added. This mixture was vortexed and centrifuged at $2,500 \times g$ at 4°C for 5 min. The process was repeated until the aqueous phase was clear. The last extraction was performed with chloroform-isoamyl alcohol to remove acid phenol. An equal volume of isopropanol was added, and the extracted nucleic acid was incubated overnight at -20°C . The following day, the sample was centrifuged at $12,000 \times g$ at 4°C for 45 min. The pellet was washed with 0°C 100% ethanol and resuspended in 200 μ l of RNase-free water. According to the manufacturer's protocol, samples were then treated with 2 μ l of Turbo DNase for 30 min at 37°C . RNA samples were retrieved using the Zymo Quick-RNA MiniPrep according to the manufacturer's protocol. The Ribo-Zero Gold rRNA removal kit (Epidemiology) was then used to deplete prokaryotic and eukaryotic rRNA from the samples according to the manufacturer's protocol (Illumina). Unstranded transcriptome sequencing (RNA-Seq) libraries were constructed with the TruSeq total RNA library preparation kit v2, both using the manufacturer's protocol. Completed libraries were stored at -20°C until time of sequencing.

High-throughput sequencing and raw read curation. Sequencing of 16S rRNA gene amplicon libraries was performed using an Illumina MiSeq sequencer as described previously (39). The 16S rRNA gene sequences were curated using the mothur software package (v1.36), and OTU-based analysis was performed as described in reference 19. Genus-level classification-based analysis of 16S rRNA gene sequence data was accomplished using the phylotype workflow in mothur and the full SILVA bacterial taxonomy (release 132). Shotgun metagenomic sequencing was performed in 2 phases. Libraries from mock-infected communities, which were also to be utilized for *de novo* contig assembly, were sequenced using an Illumina HiSeq 2500 on 2×250 paired-end settings, and sequencing was repeated across 2 lanes to normalize for interrun variation. *C. difficile*-infected metagenomic libraries were sequenced with

an Illumina NextSeq 300 with 2×150 settings across 2 runs to also normalize for interrun variation. These efforts resulted in an average of 280,000,000 paired raw reads per sample. Metatranscriptomic sequencing was performed on an Illumina HiSeq 2500 with 2×50 settings and was repeated across 4 lanes for normalization and to normalize for technical variation between lanes and to obtain necessary coverage (32). This gave an average of 380 million raw cDNA reads per library. Both metagenomic sequencing and metatranscriptomic sequencing were performed at the University of Michigan Sequencing Core. Raw sequence read curation for both metagenomic and metatranscriptomic data sets was performed in a two-step process. Residual 5' and 3' Illumina adapter sequences were trimmed using Cutadapt (41) on a per-library basis. Reads were quality trimmed using Sickle (42) with a quality cutoff of Q30. This resulted in approximately 270 million reads per library (both paired and orphaned) for both metagenomic and metatranscriptomic sequencing. Actual read abundances for individual metagenomic and metatranscriptomic sequencing efforts can be found in Table S4.

Metagenomic contig assembly and gene annotation. Metagenomic contigs were assembled using Megahit (43) with the following settings: minimum kmer size of 87, maximum kmer size of 127, and a kmer step size of 10. Prodigal was utilized to identify putative gene sequences, and sequences were screened for a minimum length of 250 nucleotides. These sequences were translated to amino acids, and the predicted peptides were annotated based on the KEGG protein database (44) using the Diamond implementation of BLASTp (45). Peptide-level gene annotations were assigned to the corresponding nucleotide sequence, and genes failing to find a match in KEGG were preserved as unannotated genes. Final nucleotide FASTA files with KEGG annotations were then utilized in the construction of Bowtie 2 mapping databases from downstream analyses (46).

DNA/cDNA read mapping and normalization. Mapping of DNA and cDNA reads to the assemblies was accomplished using Bowtie 2 and the default stringent settings (46). Optical and PCR duplicates were then removed using Picard MarkDuplicates (<http://broadinstitute.github.io/picard/>). The remaining mappings were converted to idxstats format using SAMtools (47), and the read counts per gene were tabulated. Discordant pair mappings were discarded, and counts were then normalized to read length and gene length to give a per-base report of gene coverage. Transcript abundance was then normalized to gene abundance to yield the overall level of transcription for each gene. Reads contributed by *C. difficile* were removed from analysis using Bowtie 2 against the *C. difficile* strain 630 genome with settings allowing for up to 2 mismatches.

Quantification of *in vivo* metabolite relative concentrations. Metabolomic analysis was performed by Metabolon (Durham, NC); for a detailed description of the procedure, refer to reference 19. Briefly, all methods utilized a Waters Acquity ultraperformance liquid chromatograph (UPLC) and a Thermo Scientific Q-Exactive high-resolution/accurate mass spectrometer interfaced with a heated electrospray ionization (HESI-II) source and an Orbitrap mass analyzer at 35,000-mass resolution. Samples were dried and then reconstituted in solvents compatible with each of the four methods. The first method had acidic positive conditions using a C_{18} column (Waters UPLC BEH C_{18} ; 2.1 by 100 mm, 1.7 μ m) using water and methanol, containing 0.05% perfluoropentanoic acid (PFPA) and 0.1% formic acid (FA). The second method was identical to the first but was chromatographically optimized for more hydrophobic compounds. The third approach utilized basic negative-ion-optimized conditions using a separate dedicated C_{18} column. Basic extracts were gradient eluted from the column using methanol and water but, however, with 6.5 mM ammonium bicarbonate at pH 8. Samples were then analyzed via negative ionization following elution from a hydrophilic interaction chromatography column (Waters UPLC BEH amide; 2.1 by 150 mm, 1.7 μ m) using a gradient consisting of water and acetonitrile with 10 mM ammonium formate, pH 10.8. The mass spectrometry (MS) analysis alternated between MS and data-dependent MS n scans using dynamic exclusion. The scan range varied slightly between methods but covered 70 to 1,000 m/z . Library matches for each compound were checked for each sample and corrected if necessary.

Statistical methods. All statistical analyses were performed using R (v.3.2.0) and the vegan package (48). Significant differences of inverse Simpson diversity, CFU, and metabolite concentrations were determined by Wilcoxon signed-rank test with Benjamini-Hochberg correction using a study-wide type I error rate of 0.05. Undetectable points used the limit of detection for CFU statistical calculations. Dynamic time warping was performed with the dtw package in R (49). Random Forest was performed using the AUCRF implementation (21) as well as the standard package (50) in R. Distances of outlier points from the center line during metatranscriptomic comparisons were determined using 2-dimensional linear geometry.

Data availability. Pooled and quality-trimmed *C. difficile*-infected metatranscriptomes (Sequence Read Archive [SRA] accession no. [PRJNA354635](https://www.ncbi.nlm.nih.gov/sra/PRJNA354635)) and 16S rRNA gene amplicon read data (SRA accession no. [PRJNA383577](https://www.ncbi.nlm.nih.gov/sra/PRJNA383577)) from infection experiments are available through the NCBI Sequence Read Archive. Metagenomic reads and mock-infected metatranscriptomic reads can be found also on the SRA ([PRJNA415307](https://www.ncbi.nlm.nih.gov/sra/PRJNA415307)). Data processing steps beginning with raw sequence data to the final manuscript are hosted at https://github.com/SchlossLab/Jenior_Metatranscriptomics_mSphere_2018.

SUPPLEMENTAL MATERIAL

Supplemental material for this article may be found at <https://doi.org/10.1128/mSphere.00261-18>.

FIG S1, PDF file, 0.6 MB.

FIG S2, PDF file, 1.9 MB.

FIG S3, PDF file, 0.01 MB.

FIG S4, PDF file, 0.4 MB.

TABLE S1, XLSX file, 0.01 MB.

TABLE S2, XLSX file, 0.01 MB.

TABLE S3, XLSX file, 0.01 MB.

TABLE S4, XLSX file, 0.01 MB.

ACKNOWLEDGMENTS

We acknowledge Charles Koumpouras for assistance with DNA extractions and metabolomic sample preparation. We also acknowledge members of the University of Michigan Germfree Mouse Center, University of Michigan Sequencing Core, and Metabolon for their assistance in experimental design, execution, and data collection.

M.L.J. conceived, designed, and performed experiments; analyzed data; and drafted the manuscript. J.L.L. performed experiments, analyzed data, and contributed to the manuscript. V.B.Y. contributed to the manuscript. P.D.S. interpreted data and contributed to the manuscript.

The authors declare no conflicts of interest.

REFERENCES

- Vollaard EJ, Clasener HAL. 1994. Colonization resistance. *Antimicrob Agents Chemother* 38:409–414. <https://doi.org/10.1128/AAC.38.3.409>.
- Freter R. 1955. The fatal enteric cholera infection in the guinea pig, achieved by inhibition of normal enteric flora. *J Infect Dis* 97:57–65. <https://doi.org/10.1093/infdis/97.1.57>.
- Fekety R, Silva J, Toshniwal R, Allo M, Armstrong J, Browne R, Ebricht J, Rifkin G. 1979. Antibiotic-associated colitis: effects of antibiotics on clostridium difficile and the disease in hamsters. *Rev Infect Dis* 1:386–397. <https://doi.org/10.1093/clinids/1.2.386>.
- Britton RA, Young VB. 2012. Interaction between the intestinal microbiota and host in Clostridium difficile colonization resistance. *Trends Microbiol* 20:313–319. <https://doi.org/10.1016/j.tim.2012.04.001>.
- Lessa FC, Mu Y, Bamberg WM, Beldavs ZG, Dumyati GK, Dunn JR, Farley MM, Holzbauer SM, Meek JI, Phipps EC, Wilson LE, Winston LG, Cohen JA, Limbago BM, Fridkin SK, Gerding DN, McDonald LC. 2015. Burden of Clostridium difficile infection in the United States. *N Engl J Med* 372: 825–834. <https://doi.org/10.1056/NEJMoa1408913>.
- Antonopoulos DA, Huse SM, Morrison HG, Schmidt TM, Sogin ML, Young VB. 2009. Reproducible community dynamics of the gastrointestinal microbiota following antibiotic perturbation. *Infect Immun* 77: 2367–2375. <https://doi.org/10.1128/IAI.01520-08>.
- Buffie CG, Jarchum I, Equinda M, Lipuma L, Gobourne A, Viale A, Ubeda C, Xavier J, Pamer EG. 2012. Profound alterations of intestinal microbiota following a single dose of clindamycin results in sustained susceptibility to Clostridium difficile-induced colitis. *Infect Immun* 80:62–73. <https://doi.org/10.1128/IAI.05496-11>.
- Thomas C, Stevenson M, Riley TV. 2003. Antibiotics and hospital-acquired Clostridium difficile-associated diarrhoea: a systematic review. *J Antimicrob Chemother* 51:1339–1350. <https://doi.org/10.1093/jac/dkg254>.
- Brown KA, Khanafer N, Daneman N, Fisman DN. 2013. Meta-analysis of antibiotics and the risk of community-associated Clostridium difficile infection. *Antimicrob Agents Chemother* 57:2326–2332. <https://doi.org/10.1128/AAC.02176-12>.
- Bignardi GE. 1998. Risk factors for Clostridium difficile infection. *J Hosp Infect* 40:1–15. [https://doi.org/10.1016/S0195-6701\(98\)90019-6](https://doi.org/10.1016/S0195-6701(98)90019-6).
- Antunes LCM, Han J, Ferreira RBR, Lolić P, Borchers CH, Finlay BB. 2011. Effect of antibiotic treatment on the intestinal metabolome. *Antimicrob Agents Chemother* 55:1494–1503. <https://doi.org/10.1128/AAC.01664-10>.
- Jump RLP, Polinkovsky A, Hurless K, Sitzlar B, Eckart K, Tomas M, Deshpande A, Nerandzic MM, Donskey CJ. 2014. Metabolomics analysis identifies intestinal microbiota-derived biomarkers of colonization resistance in clindamycin-treated mice. *PLoS One* 9:e101267. <https://doi.org/10.1371/journal.pone.0101267>.
- Theriot CM, Koenigsnecht MJ, Carlson PE, Hatton GE, Nelson AM, Li B, Huffnagle GB, Li JZ, Young VB. 2014. Antibiotic-induced shifts in the mouse gut microbiome and metabolome increase susceptibility to Clostridium difficile infection. *Nat Commun* 5:3114. <https://doi.org/10.1038/ncomms4114>.
- Wilson KH, Perini F. 1988. Role of competition for nutrients in suppression of Clostridium difficile by the colonic microflora. *Infect Immun* 56:2610–2614.
- Sambol SP, Merrigan MM, Tang JK, Johnson S, Gerding DN. 2002. Colonization for the prevention of Clostridium difficile disease in hamsters. *J Infect Dis* 186:1781–1789. <https://doi.org/10.1086/345676>.
- Pérez-Cobas AE, Artacho A, Ott SJ, Moya A, Gosalbes MJ, Latorre A. 2014. Structural and functional changes in the gut microbiota associated to Clostridium difficile infection. *Front Microbiol* 5:335. <https://doi.org/10.3389/fmicb.2014.00335>.
- Zaura E, Brandt BW, Teixeira de Mattos MJT, Buijs MJ, Caspers MPM, Rashid MU, Weintraub A, Nord CE, Savell A, Hu Y, Coates AR, Hubank M, Spratt DA, Wilson M, Keijsers BJF, Crielaard W. 2015. Same exposure but two radically different responses to antibiotics: resilience of the salivary microbiome versus long-term microbial shifts in feces. *mBio* 6:e01693-15. <https://doi.org/10.1128/mBio.01693-15>.
- Schubert AM, Sinani H, Schloss PD. 2015. Antibiotic-induced alterations of the murine gut microbiota and subsequent effects on colonization resistance against Clostridium difficile. *mBio* 6:e00974-15. <https://doi.org/10.1128/mBio.00974-15>.
- Jenior ML, Leslie JL, Young VB, Schloss PD. 2017. Clostridium difficile colonizes alternative nutrient niches during infection across distinct murine gut microbiomes. *mSystems* 2:e00063-17. <https://doi.org/10.1128/mSystems.00063-17>.
- Koenigsnecht MJ, Theriot CM, Bergin IL, Schumacher CA, Schloss PD, Young VB. 2015. Dynamics and establishment of Clostridium difficile infection in the murine gastrointestinal tract. *Infect Immun* 83:934–941. <https://doi.org/10.1128/IAI.02768-14>.
- Calle ML, Urrea V, Boulesteix AL, Malats N. 2011. AUC-RF: a new strategy for genomic profiling with random forest. *Hum Hered* 72:121–132. <https://doi.org/10.1159/000330778>.
- Fletcher JR, Erwin S, Lanzas C, Theriot CM. 2018. Shifts in the gut metabolome and Clostridium difficile transcriptome throughout colonization and infection in a mouse model. *mSphere* 3:e00089-18. <https://doi.org/10.1128/mSphere.00089-18>.
- Dai Z, Wu Z, Hang S, Zhu W, Wu G. 2015. Amino acid metabolism in intestinal bacteria and its potential implications for mammalian reproduction. *Mol Hum Reprod* 21:389–409. <https://doi.org/10.1093/molehr/gav003>.
- Bouillaut L, Dubois T, Sonenshein AL, Dupuy B. 2015. Integration of metabolism and virulence in Clostridium difficile. *Res Microbiol* 166: 375–383. <https://doi.org/10.1016/j.resmic.2014.10.002>.
- Mahowald MA, Rey FE, Seedorf H, Turnbaugh PJ, Fulton RS, Wollam A, Shah N, Wang C, Magrini V, Wilson RK, Cantarel BL, Coutinho PM, Henrissat B, Crock LW, Russell A, Verberkmoes NC, Hettich RL, Gordon JI. 2009. Characterizing a model human gut microbiota composed of members of its two dominant bacterial phyla. *Proc Natl Acad Sci U S A* 106:5859–5864. <https://doi.org/10.1073/pnas.0901529106>.
- Jousset A, Bienhold C, Chatzinotas A, Gallien L, Gobet A, Kurm V, Küsel

- K, Rillig MC, Rivett DW, Salles JF, van der Heijden MGA, Youssef NH, Zhang X, Wei Z, Hol WHG. 2017. Where less may be more: how the rare biosphere pulls ecosystems strings. *ISME J* 11:853–862. <https://doi.org/10.1038/ismej.2016.174>.
27. Shade A, Jones SE, Caporaso JG, Handelsman J, Knight R, Fierer N, Gilbert JA. 2014. Conditionally rare taxa disproportionately contribute to temporal changes in microbial diversity. *mBio* 5:e01371-14. <https://doi.org/10.1128/mBio.01371-14>.
 28. Rojo D, Gosalbes MJ, Ferrari R, Pérez-Cobas AE, Hernández E, Oltra R, Buesa J, Latorre A, Barbas C, Ferrer M, Moya A. 2015. *Clostridium difficile* heterogeneously impacts intestinal community architecture but drives stable metabolome responses. *ISME J* 9:2206–2220. <https://doi.org/10.1038/ismej.2015.32>.
 29. Abraham NM, Liu L, Jutras BL, Yadav AK, Narasimhan S, Gopalakrishnan V, Ansari JM, Jefferson KK, Cava F, Jacobs-Wagner C, Fikrig E. 2017. Pathogen-mediated manipulation of arthropod microbiota to promote infection. *Proc Natl Acad Sci U S A* 114:E781–E790. <https://doi.org/10.1073/pnas.1613422114>.
 30. Russel J, Røder HL, Madsen JS, Burmølle M, Sørensen SJ. 2017. Antagonism correlates with metabolic similarity in diverse bacteria. *Proc Natl Acad Sci U S A* 114:10684–10688. <https://doi.org/10.1073/pnas.1706016114>.
 31. Sheik CS, Jain S, Dick GJ. 2014. Metabolic flexibility of enigmatic SAR324 revealed through metagenomics and metatranscriptomics. *Environ Microbiol* 16:304–317. <https://doi.org/10.1111/1462-2920.12165>.
 32. Franzosa EA, Morgan XC, Segata N, Waldron L, Reyes J, Earl AM, Gianoukos G, Boylan MR, Ciulla D, Gevers D, Izard J, Garrett WS, Chan AT, Huttenhower C. 2014. Relating the metatranscriptome and metagenome of the human gut. *Proc Natl Acad Sci U S A* 111:E2329–E2338. <https://doi.org/10.1073/pnas.1319284111>.
 33. Jorth P, Turner KH, Gumus P, Nizam N, Buduneli N, Whiteley M. 2014. Metatranscriptomics of the human oral microbiome during health and disease. *mBio* 5:e01012-14. <https://doi.org/10.1128/mBio.01012-14>.
 34. Reeves AE, Koenigsnecht MJ, Bergin IL, Young VB. 2012. Suppression of *Clostridium difficile* in the gastrointestinal tracts of germfree mice inoculated with a murine isolate from the family Lachnospiraceae. *Infect Immun* 80:3786–3794. <https://doi.org/10.1128/IAI.00647-12>.
 35. Lawley TD, Clare S, Walker AW, Stares MD, Connor TR, Raisen C, Goulding D, Rad R, Schreiber F, Brandt C, Deakin LJ, Pickard DJ, Duncan SH, Flint HJ, Clark TG, Parkhill J, Dougan G. 2012. Targeted restoration of the intestinal microbiota with a simple, defined bacteriotherapy resolves relapsing *Clostridium difficile* disease in mice. *PLoS Pathog* 8:e1002995. <https://doi.org/10.1371/journal.ppat.1002995>.
 36. Petrof EO, Gloor GB, Vanner SJ, Weese SJ, Carter D, Daigneault MC, Brown EM, Schroeter K, Allen-Vercoe E. 2013. Stool substitute transplant therapy for the eradication of *Clostridium difficile* infection: ‘RePOOPulating’ the gut. *Microbiome* 1:3. <https://doi.org/10.1186/2049-2618-1-3>.
 37. Buffie CG, Bucci V, Stein RR, McKenney PT, Ling L, Gobourne A, Liu H, Kinnebrew M, Viale A, Littmann E, van den Brink MR, Jenq RR, Taur Y, Sander C, Cross JR, Toussaint NC, Xavier JB, Pamer EG. 2015. Precision microbiome reconstitution restores bile acid mediated resistance to *Clostridium difficile*. *Nature* 517:205–208. <https://doi.org/10.1038/nature13828>.
 38. Wilson KH, Kennedy MJ, Fekety FR. 1982. Use of sodium taurocholate to enhance spore recovery on a medium selective for *Clostridium difficile*. *J Clin Microbiol* 15:443–446.
 39. Kozich J, Westcott S, Baxter N, Highlander S, Schloss P. 2013. 16S sequencing with the Illumina MiSeq personal sequencer, p 1–16. *In* University of Michigan Health System standard operating procedure. University of Michigan, Ann Arbor, MI.
 40. Lopez-Medina E, Neubauer MM, Pier GB, Koh AY. 2011. RNA isolation of *Pseudomonas aeruginosa* colonizing the murine gastrointestinal tract. *J Vis Exp* 55:e3293. <https://doi.org/10.3791/3293>.
 41. Martin M. 2011. Cutadapt removes adapter sequences from high-throughput sequencing reads. *EMBnet J* 17:10. <https://doi.org/10.14806/ej.17.1.200>.
 42. Joshi N, Fass J. 2011. Sickle: a sliding-window, adaptive, quality-based trimming tool for FastQ files (version 1.33). <https://github.com/najoshi/sickle>.
 43. Li D, Liu CM, Luo R, Sadakane K, Lam TW. 2015. MEGAHIT: an ultra-fast single-node solution for large and complex metagenomics assembly via succinct de Bruijn graph. *Bioinformatics* 31:1674–1676. <https://doi.org/10.1093/bioinformatics/btv033>.
 44. Ogata H, Goto S, Sato K, Fujibuchi W, Bono H, Kanehisa M. 1999. KEGG: Kyoto encyclopedia of genes and genomes. *Nucleic Acids Res* 27:29–34. <https://doi.org/10.1093/nar/27.1.29>.
 45. Buchfink B, Xie C, Huson DH. 2015. Fast and sensitive protein alignment using DIAMOND. *Nat Methods* 12:59–60. <https://doi.org/10.1038/nmeth.3176>.
 46. Langmead B, Salzberg SL. 2012. Fast gapped-read alignment with Bowtie 2. *Nat Methods* 9:357–359. <https://doi.org/10.1038/nmeth.1923>.
 47. Li H, Handsaker B, Wysoker A, Fennell T, Ruan J, Homer N, Marth G, Abecasis G, Durbin R, 1000 Genome Project Data Processing Subgroup. 2009. The Sequence Alignment/Map format and SAMtools. *Bioinformatics* 25:2078–2079. <https://doi.org/10.1093/bioinformatics/btp352>.
 48. Oksanen J, Blanchet FG, Friendly M, Kindt R, Legendre P, McGlenn D, Minchin PR, O’Hara RB, Simpson GL, Solymos P, Stevens MHH, Szoecs E, Wagner H. 2018. Vegan: community ecology package.
 49. Giorgino T. 2009. Computing and visualizing dynamic time warping alignments in R: the dtw package. *J Stat Softw* 31:1–24. <https://doi.org/10.18637/jss.v031.i07>.
 50. Breiman L. 2001. Random forests. *Mach Learn* 45:5–32. <https://doi.org/10.1023/A:1010933404324>.